Proper chromosome alignment depends on BRCA2 phosphorylation by PLK1

Åsa Ehlén[1,2], Charlotte Martin[1,2†], Manon Julien[3,4†], Simona Miron[3†], François-Xavier Theillet[3], Virginie Boucherit[1,2], Patricia Duchambon[5,6], Ahmed El Marjou[5,7], Sophie Zinn-Justin[3], Aura Carreira[1,2,*]

[1]Institut Curie, PSL Research University, CNRS, UMR3348, F-91405, Orsay, France

[2]Paris Sud University, Paris-Saclay University CNRS, UMR3348, F-91405 Orsay, France

[3]Institute for Integrative Biology of the Cell (I2BC), CEA, CNRS, Univ Paris-Sud, Université Paris-Saclay, Gif-sur-Yvette Cedex, France

[4]Department of Biology, École Normale Supérieure, 94230 Cachan, France
[5]Protein Expression and Purification Core Facility, Institut Curie, 26 rue d'Ulm, 75248 Paris Cedex 05, France
[6]INSERM U1196, 91405 Orsay Cedex, France
[7]CNRS UMR144, 12 rue Lhomond, 75005 Paris, France

[†] Equal contributors

[*]To whom correspondence should be addressed:
Aura Carreira
Institut Curie - Research Center
UMR 3348 CNRS "Genotoxic Stress and Cancer"
Bâtiment 110, Centre Universitaire
91405 Orsay
France
Phone: +33 (0)1 69 86 30 82
Fax: +33 (0)1 69 86 94 29
E-mail: aura.carreira@curie.fr

Summary

The BRCA2 tumor suppressor protein is involved in the maintenance of genome integrity through its role in homologous recombination (HR) in S/G2 phases of the cell cycle. In mitosis, BRCA2 participates in the spindle assembly checkpoint (SAC) via its interaction with the SAC component BUBR1 and is involved in cytokinesis. Also in mitosis, BRCA2 is phosphorylated by the cell cycle regulator Polo-like kinase 1 (PLK1), although the functional relevance of this phosphorylation remains unclear. Here we combine nuclear magnetic resonance spectroscopy, isothermal titration calorimetry and cell biology to characterize the phenotype of *BRCA2* variants that alter PLK1 phosphorylation. We identify T207 of BRCA2 as a *bona fide* docking site for PLK1 required for the phosphorylation of BUBR1 and the proper alignment of the chromosomes at the metaphase plate. Precluding T207 binding to PLK1 as observed in *BRCA2* missense variants identified in breast cancer results in reduced phosphorylation of BUBR1 at PLK1-dependent sites leading to severe chromosome misalignment and segregation errors. We thus reveal a control mechanism of chromosome alignment that depends on the PLK1-BRCA2 interaction.

Keywords

BRCA2; variants of uncertain significance (VUS); PLK1; Phosphorylation; chromosome alignment; BUBR1; Mitosis

Introduction

BRCA2 tumor suppressor plays an important role in DNA repair by homologous recombination[1,2] which takes place preferentially during S/G2 phases of the cell cycle[3]. In mitosis, BRCA2 interacts with the acetyl transferase PCAF[4] and the spindle assembly component BUBR1[5], facilitating the acetylation of the latter, which provides evidence for a role of BRCA2 in the spindle assembly checkpoint (SAC)[6]. BRCA2 also localizes to the midbody and facilitates cell division by serving as a scaffold protein for the central spindle components[7-9]. Also in mitosis, BRCA2 is phosphorylated by PLK1 both in its N-terminal region[10] and in its central region[11], although the functional role of these phosphorylation events remains unclear.

PLK1 is a master regulator of the cell cycle, especially in mitosis[12,13]. Among other functions, PLK1 phosphorylates BUBR1 at several residues including the tension-sensitive T680[14] and S676[15] in prometaphase allowing the formation of stable kinetochore-microtubule attachments. This activity needs to be tightly regulated to ensure the proper alignment of the chromosomes at the metaphase plate[15-17].

PLK1 is recruited to specific targets via its Polo-box domain (PBD) [18]. PBD interacts with phosphosites characterized by the consensus motif S-[pS/pT]-P/X[19]. These phosphosites are provided by a priming phosphorylation event, usually mediated by CDK1 or other proline-directed kinases[13]; there is also evidence that PLK1 itself might create docking sites during cytokinesis [20,21].

Several BRCA2 sites corresponding to PLK1 consensus motifs have been identified as phosphorylated in mitosis, some of which belong to a cluster of predicted phosphosites located in BRCA2 N-terminus around residue S193[10]. We set out to investigate which of these sites are phosphorylated by PLK1, and to reveal whether these phosphorylation events play a role in the regulation of mitotic progression.

Here, we demonstrate that T207 is a *bona fide* docking site for PLK1. By investigating the phenotype of BRCA2 missense variants that limit the phosphorylation of T207 by PLK1 we reveal an unexpected role for BRCA2 in the alignment of chromosomes at the metaphase plate. Furthermore, we provide evidence that this function is achieved by promoting the phosphorylation of the kinetochore tension-sensitive sites of BUBR1 by PLK1.

Results

BRCA2 variants identified in breast cancer reduce the PLK1-dependent phosphorylation of BRCA2 N-terminal region

Several missense variants of uncertain significance (VUS) identified in *BRCA2* in breast cancer patients are located in the region predicted to be phosphorylated by PLK1 (around S193) (Breast information core (BIC)[22] and BRCAshare [23]). To find out if any of these variants affected PLK1 phosphorylation in this region, we expressed and purified a maltose binding protein (MBP)-tagged version of a fragment comprising aa 1-250, hereafter $BRCA2_{1-250}$, from human HEK293T cells containing either wild-type (WT), VUS M192T, S196N, T200K, S206C and T207A, or the mutant S193A (Figure 1a), the latter being previously described as reducing phosphorylation of BRCA2 by PLK1[10]. Using an *in vitro* kinase assay, we assessed the phosphorylation by PLK1 of the $BRCA2_{1-250}$ fragment containing each mutation and compared it to the WT protein (Figure 1b). As reported before, S193A reduced phosphorylation of $BRCA2_{1-250}$ by PLK1 (Figures 1b and 1c). Interestingly, variants T207A, S206C and T200K led to a 2-fold decrease in PLK1 phosphorylation of $BRCA2_{1-250}$ (Figures 1b and 1c). In contrast, M192T slightly increased the

phosphorylation above WT levels whereas VUS S196N did not significantly modify the phosphorylation of $BRCA2_{1-250}$ by PLK1 (Figures 1b, c).

Together, these results show that VUS T207A, S206C and T200K identified in breast cancer patients impair phosphorylation of $BRCA2_{1-250}$ by PLK1 *in vitro*.

$BRCA2_{T207}$ is a target of phosphorylation by PLK1

The reduction of BRCA2 phosphorylation in $BRCA2_{1-250}$T207A and S206C suggested that T207 could be a target of PLK1 phosphorylation. We investigated this possibility by following the phosphorylation kinetics of a truncated fragment of BRCA2 N-terminus comprising T207 (amino acids 190-283) (hereafter $BRCA2_{190-283}$). We used Nuclear Magnetic Resonance (NMR) spectroscopy to monitor $BRCA2_{190-283}$ phosphorylation by recombinant PLK1 *in vitro*. NMR analysis allows residue-specific quantification of a peptide modification, provided it is ^{15}N-labelled. Figure 2a shows superimposed ^{1}H-^{15}N HSQC spectra of $BRCA2_{190-283}$ at different time points of the phosphorylation reaction by PLK1. Analysis of these experiments revealed phosphorylation of S193 and of eight other phosphosites, among which three threonines and five serines (Figure 2a). Four residues (T226>T207>T219>S193, Figure 2b, S1a) were favoured phosphorylation sites, modified with markedly faster rates than the five other sites (S197, S217, S231, S239, S273). Interestingly, while T219 and T226 conservation is poor, T207 and S193 are conserved from mammals to fishes (Figures S1b and S1c) suggesting that both are important for BRCA2 function.

The phosphorylation of T207 together with the presence of a serine residue at position 206 creates a predicted docking site for $PLK1_{PBD}$[19]. Hence, we conclude that T207 phosphorylation by PLK1 is efficient in the context of $BRCA2_{190-283}$, and it may

be a primary event for further BRCA2 phosphorylation via the recruitment of PLK1 to BRCA2.

BRCA2 variants T207A and T200K alter the phosphorylation kinetics of PLK1

Having identified T207 as a target of phosphorylation of PLK1, we next assessed the phosphorylation kinetics of T207 in the WT $BRCA2_{190-283}$ fragment and in the fragment containing the variants T207A or T200K that displayed reduced phosphorylation (Figure 1b, c). Time-resolved NMR experiments revealed that PLK1 phosphorylates significantly less $BRCA2_{190-283}$ containing the variant T207A than the WT peptide (Figure 3a, 3b). Initial phosphorylation rates were decreased by a factor 5 (S193), 8 (T226) and 13 (T219) (Figure 3b, S2a). Variant T200K reduced by half the phosphorylation rates of S193, T207, T219 and T226 (Figures 3c, 3d and S2b).

In agreement with the *in vitro* kinase assay using the $BRCA2_{1-250}$ fragment purified from human cells (Figure 1), these results show that in $BRCA2_{190-283}$, variants T207A and T200K identified in breast cancer patients impair the phosphorylation of T207 and the cascade of associated phosphorylation events.

VUS T207A, S206C and T200K reduce the interaction of BRCA2 and PLK1

The finding that T207 is efficiently phosphorylated by PLK1 in $BRCA2_{190-283}$ polypeptide (Figure 2a) together with the observation that T207A mutation causes a global decrease in the phosphorylation of this region (Figure 3a) and the prediction that T207 is a docking site for $PLK1_{PBD}$ binding[19] made us hypothesize that T207 might be a “self-priming” phosphorylation event required for the interaction of PLK1 with BRCA2 at this site. The variants that reduce phosphorylation of T207 by PLK1 would then be predicted to alter $PLK1_{PBD}$ binding. To test this hypothesis, we

examined the interaction of PLK1 with the VUS containing polypeptides. Using an amylose pull-down, we overexpressed 2xMBP-BRCA2$_{1-250}$ constructs carrying these variants in U2OS cells and detected the bound endogenous PLK1 by western blotting. As expected, overexpressed BRCA2$_{1-250}$ was able to interact with endogenous PLK1 from mitotic cells but not from asynchronous cells (Figure 4a, lane 2 compared to lane 1). As previously described, [10], mutation S193A reduced the binding to PLK1 (Figure 4a, lane 6 compared to lane 2). Interestingly, the variants reducing PLK1 phosphorylation (T207A, S206C and T200K) showed a weaker interaction with PLK1 than the WT protein (Figure 4a pull-down lane 4, 8 compared to lane 2 and lane 20 compared to lane 18) despite the protein levels of PLK1 being unchanged (Figure 4a, compare PLK1 input lanes 2, 4, 6, 8, 18, 20); in contrast, M192T and S196N did not affect the binding (Figure 4a, pull-down lane 12, 14 compared to lane 10). These results are consistent with the idea of a self-priming phosphorylation by PLK1 on T207.

T207 is a *bona fide* docking site for PLK1

To directly prove the recognition of pT207 by PLK1, we measured the affinity of recombinant PLK1$_{PBD}$ for a synthetic 17 aa peptide comprising phosphorylated T207. Using isothermal titration calorimetry (ITC), we found that recombinant PLK1$_{PBD}$ bound to the T207 phosphorylated peptide with an affinity of K_d= 0.09 ± 0.07 μM (Figure 4b), similar to the optimal affinity reported for an interaction between PLK1$_{PBD}$ and its phosphorylated target[19]. Consistently, PLK1$_{PBD}$ bound to the fragment BRCA2$_{190-283}$ with a micromolar affinity upon phosphorylation by PLK1 (K_d= 0.14 ± 0.02 μM; Figure S3a) whereas it did not bind to the corresponding non-phosphorylated polypeptides (Figure 4c, Figure S3b). In

agreement with the pull-down experiments, a peptide comprising mutated T207A abolished the interaction (Figure 4d). Importantly, a peptide comprising pT207 and S206C mutation could not bind to $PLK1_{PBD}$ (Figure 4e), as predicted from the consensus sequence requirement for $PLK1_{PBD}$ interaction[19]. Last, a peptide containing phosphorylated S197, which is also a predicted docking site for PLK1, bound with much less affinity to $PLK1_{PBD}$ than pT207 (K_d= 17 ± 2 µM; Figure S3c).

Taken together, these results indicate that phosphorylation of T207 by PLK1 promotes the interaction of PLK1 with BRCA2 through a *bona fide* docking site for PLK1 and favours a cascade of phosphorylation events. In variants T200K and T207A the decrease in T207 phosphorylation impairs PLK1 docking at T207 explaining the reduction of binding to PLK1 and the global loss of phosphorylation by PLK1. S206C eliminates the serine residue at -1 required for $PLK1_{PBD}$ interaction resulting as well in a reduction of BRCA2 binding.

Impairing T207 phosphorylation delays mitosis

PLK1 is a master regulator of mitosis[13]. To find out whether the interaction between BRCA2 and PLK1 is involved in the control of mitotic progression we examined the functional impact of two of the variants that reduce PLK1 phosphorylation at T207 (S206C and T207A) in the context of the full-length BRCA2 protein in cells. For this purpose, we generated stable clones expressing the cDNA coding of either the WT or the variants full-length BRCA2 to complement the knock out *BRCA2* cell line $DLD1^{-/-}$[24]. We selected two clones for each variant showing similar protein levels as the WT clone (Figure S4a).

To examine the impact of these variants on mitosis, we monitored by time-lapse microscopy the time that double-thymidine-synchronized individual cells from each

clone spent in mitosis, from mitotic entry to daughter cell separation. DLD1$^{+/+}$ and the WT clone showed similar kinetics, the majority of the cells (67% for DLD1$^{+/+}$ and 83% for the WT clone) having completed mitosis within 60 min (Figure 5a, 5b). In contrast, cells expressing variants S206C and T207A augmented the time spent in mitosis as manifested by a significant decrease in the frequency of cells dividing within 60 min (~50%), similar to the BRCA2 deficient cells (DLD$^{-/-}$) (Figures 5a and 5b). In addition to a slower mitotic progression, S206C and T207A showed higher frequency of mitotic failure than WT (14-23% compared to ~4% for the WT clone) (Figure 5a, failure).

As depletion of BRCA2 has been shown to impair SAC activity [6], we next assessed the SAC activity by measuring the percentage of cells arrested in mitosis after treatment with the spindle poison nocodazole (Figure 5c), using phosphorylated (S10) histone 3 (pH3) as a mitotic marker[25]. As expected, upon nocodazole treatment, the percentage of pH3 positive WT cells increased compared to non-treated cells, this increase was similar to the one observed in cells expressing endogenous BRCA2 (DLD$^{+/+}$) whereas in BRCA2 deficient cells (DLD$^{-/-}$) the percentage was significantly lower (Figure 5c). Interestingly, the stable cell lines expressing variants S206C and T207A showed a significant decrease in the percentage of mitotic cells after nocodazole treatment in comparison to the WT cells, indicating a weaken SAC activity under mitotic-arrested conditions (Figure 5c). Consistently, a smaller percentage of G2/M cells was observed in S206C and T207A clones compared to the WT clone upon mitotic arrest induction (Figure S4b). The reduced number of cells in G2/M was not due to a defective cell cycle profile as the distribution of these cells in non-induced conditions was equivalent to that of the WT cells (Figure S4c).

Taken together, cells expressing S206C and T207A display slower mitotic progression and higher frequency of mitotic failure compared to WT cells. In response to microtubule poison, VUS S206C and T207A compromise SAC activity, which results in a weaken ability to induce mitotic arrest.

Docking of PLK1 at T207 of BRCA2 promotes phosphorylation of BUBR1 at T680 and S676 by PLK1

BRCA2 interacts directly with BUBR1[5,6]. BUBR1 associates with and is phosphorylated by PLK1, which controls the stability of kinetochore-microtubule interactions and enables the alignment of chromosomes at the metaphase plate[14,15]. The defective mitotic progression observed in the clones expressing S206C and T207A (Figure 5a, b) led us to investigate BUBR1 levels in these cell lines. As previously described[15,26], upon cell arrest in G2/M phase, BUBR1 displayed 2 bands, the up-shifted band corresponding to phosphorylated BUBR1 (Figure 6a). Interestingly, the up-shifted band of BUBR1 strongly decreased in the cells expressing variants S206C or T207A compared to the cells expressing WT BRCA2 (Figure 6a). To find out the species of BUBR1 altered in the clones, we probed the same membrane with an antibody specific for pT680, a known BUBR1 target phosphosite for PLK1[14]. Interestingly, both clones of the cells expressing variants S206C and T207A displayed reduced pT680 levels of BUBR1 (Figure 6a). As previously described[14], the phosphorylation of T680 is mediated by PLK1 since PLK1 inhibitors strongly reduced this signal (Figure S4d) and phosphatase treatment resulted in a decrease of the intensity of the band (Figure S4e). Furthermore, we observed a reduction in the PLK1-dependent phosphorylation of S676, another

known target site of PLK1 in BUBR1[15] (Figure 6b), suggesting that BUBR1 phosphorylation by PLK1 is impaired in these cells.

Together, our results show that BUBR1 phosphorylation by PLK1 is impaired in cells expressing the variants of BRCA2 that cannot recruit PLK1 at T207.

Variants of BRCA2 that reduce PLK1 phosphorylation display strong chromosome misalignments

The phosphorylation of BUBR1 at T680 and S676 by PLK1 has been implicated in the formation of stable kinetochore-microtubules attachments[14,15], a defect of which results in chromosome misalignment. Therefore, we next examined whether cells expressing the BRCA2 variant T207A that showed reduced levels of pT680 and pS676-BUBR1 altered chromosome alignment.

Following thymidine synchronization, the cells were blocked in prometaphase with monastrol and then treated with proteasome inhibitor MG132 for 1h to avoid exit from mitosis. Chromosome alignment was subsequently analysed by immunofluorescence.

Importantly, analysis of metaphase cells in the two cell clones of the T207A variant showed high frequency of chromosome misalignments compared to the WT BRCA2 clone (27% in T207 E4 and 35% in T207 B1 versus 13.9% in the WT clone) (Figure 6c, d) as detected by a signal of the centromere marker (CREST) outside the metaphase plate (Figure 6d). Strikingly, as opposed to the WT clone, most of the misaligned chromosomes in the cells expressing the T207A variant were located close to the spindle pole revealed by staining with the microtubule marker alpha-tubulin (Figure 6c, 6d).

Unresolved chromosome misalignment can lead to chromosome missegregation. To find out if this was the case in cells expressing S206C and T207A variants we next examined these cells at anaphase/telophase upon nocodazole-induced mitotic arrest. As quantified in Figure 7a and illustrated in Figure 7b, all cells expressing both clones of S206C and T207A variants displayed increased chromosome segregation errors including lagging chromosomes and chromatin bridges, although the difference in clone T207A E4 was not statistically significant probably due to the higher expression levels of mutated BRCA2 in this variant (Figure S4a).

These results indicate that precluding the docking of PLK1 at T207 in BRCA2 is enough to impair BUBR1 phosphorylation by the same kinase. The outcome is the one expected for BUBR1 phosphorylation impairment[15,17] i.e., chromosome misalignment and chromosome missegregation (Figures 6c, d and 7a, b).

Variants altering PLK1 phosphorylation do not affect the DNA repair activity of BRCA2

Since BRCA2 has a major role in DNA repair by homologous recombination (HR), the delayed mitosis observed in the VUS clones could result from checkpoint activation through unrepaired DNA. To rule out this possibility, we treated the stable clones with mitomycin C (MMC) and performed a clonogenic cell survival assay. As expected, the DLD1$^{-/-}$ cells showed hypersensitivity to the treatment whereas the WT clone complemented this phenotype almost to the same survival levels as the DLD1$^{+/+}$ cells carrying the endogenous BRCA2, validating our cell system. Similarly, the stable clones expressing VUS S206C and T207A also complemented the hypersensitive phenotype (Figure 7c) suggesting that the delay in mitosis is not a consequence of checkpoint activation via unrepaired DNA. In contrast, clones

expressing VUS S206C and T207A did show a growth defect manifested in a reduced number of colonies observed in unchallenged cells (Figure 7d), which is consistent with the mitotic delay observed in the video-microscopy experiment (Figure 5a, 5b). Moreover, the interaction of $BRCA2_{1-250}$ and PLK1 was not affected by IR treatment in mitosis (Figure 7d) consistent with previous work [27] suggesting that their interaction in mitosis is independent of the HR function of BRCA2.

Discussion

Our results demonstrate that residues S193 and T207 of BRCA2 can be phosphorylated by PLK1 (Figure 2) and that pT207 constitutes a *bona fide* docking site for $PLK1_{PBD}$ (Figure 4b). Accordingly, *BRCA2* missense variants of unknown clinical significance reducing the phosphorylation status of T207 (T207A, S206C, T200K), result in a decrease in the interaction of BRCA2-PLK1 (Figure 4). The phenotype of cells expressing two of these variants (S206C, T207A) in the context of the full-length protein in BRCA2 deficient background, allowed us to investigate in detail the role of BRCA2 phosphorylation by PLK1 in mitosis that was until now unclear. We found that the BRCA2 missense variants precluding the docking of PLK1 at T207 results in severe chromosome misalignments (Figure 6c, d). Remarkably, the variant T207A of BRCA2 leads to a frequency of chromosome misalignment equivalent to the one reported for BUBR1 T680A mutant[14].

Mechanistically, cells expressing T207A and S206C exhibit reduced PLK1-dependent BUBR1 phosphorylation at both known tension-sensitive phosphosites required for the establishment of kinetochore-microtubule attachments (Figure 6a, b)[14,15]. Importantly, these results suggest that the recruitment of PLK1 at pT207

docking site in BRCA2 permits the phosphorylation of BUBR1 by PLK1.

The consequences of the increased chromosome misalignments are mitotic delay, weaken SAC activity upon induced mitotic arrest, chromosome missegregation and increased cytokinetic failure (Figure 5, 7a, b).

Finally, the activity of BRCA2-PLK1 interaction in mitotic progression is independent of the HR function of BRCA2 as cells expressing these VUS display normal sensitivity to DNA damage (Figure 7c).

Putting our results together we propose the following model (Figure 7f). In BRCA2 WT cells PLK1 phosphorylates BRCA2 on T207 which leads to the docking of PLK1 at pT207 on BRCA2 supporting the phosphorylation of BUBR1 at the tension-sensitive phosphosites (T680 and S676) by PLK1 in prometaphase. Once the kinetochore-microtubules attachments are established and proper tension is achieved, BUBR1 is no longer phosphorylated by PLK1[15]. This leads to a full alignment of chromosomes at the metaphase plate (Figure 7f, panel 2) and the subsequent faithful chromosome segregation in anaphase (Figure 7f, panel 3).

In cells expressing the variants that fail to be phosphorylated at T207 (T200K, S206C, T207A) PLK1 cannot be recruited to pT207, impairing the phosphorylation of BUBR1 by the same kinase, thus leading to misalignment defects that prolong mitosis (Figure 7f, panel 2'). This may also unbalance the pool of BUBR1 required for SAC activation as cells carrying these variants display weaken SAC response only upon treatment with microtubule poison (Figure 5a); as a consequence, these cells exhibit increased chromosome segregation errors (Figure 7f, panel 3') and mitotic failure. The phenotype we observe in these clones fits very well with the presence of two pools of BUBR1 as recently described [17], one that is important for chromosome

alignment onto the metaphase plate, and another that activates the SAC.

Our results are consistent with the "processive phosphorylation" model (as opposed to the "distributive phosphorylation" model) proposed before on how $PLK1_{PBD}$ regulates the kinase activity of PLK1[28], with some modifications. In this model, $PLK1_{PBD}$ would bind first the site phosphorylated by another mitotic kinase and then the kinase domain of PLK1 would be positioned to phosphorylate the same protein at another site. In this work, we show that the mitotic kinase would be PLK1 itself ("self-priming"[21]), and the kinase domain of PLK1 would phosphorylate not the same protein but BUBR1 presumably bound to BRCA2. This model is also consistent with the fact that BRCA2 localization to the kinetochore is dependent on PLK1 activity as recently shown[29], discarding that BRCA2 recruits PLK1 to the kinetochore (distributive phosphorylation model[28]).

In all, we reveal a PLK1 self-priming docking site at BRCA2 pT207 that favours BUBR1 phosphorylation by the same kinase facilitating full chromosome alignment.

BRCA2 also supports the acetylation of BUBR1 which appears to be necessary for SAC silencing[6]; how these BUBR1 acetylation and phosphorylation events are coordinated in mitosis is still unclear. Moreover, BRCA2 harbours another docking site for PLK1 at T77, a site that is primed by CDK phosphorylation[27]. In addition to T207, we have observed other phosphorylation events including S193 (Figure 2), required for the midbody localization of BRCA2[9], and there are other PLK1-phosphorylation sites described in the central region of the protein[11]. What is the chronology of phosphorylation events throughout the cell cycle and how they are regulated deserves further study.

The fact that *BRCA2* missense variants identified in breast cancer patients affect

BRCA2 phosphorylation by PLK1 with direct consequences in chromosome alignment and segregation suggests that this function could be associated with the aneuploidy observed in *BRCA2*-deficient tumors.

Author Contributions

A.E. purified WT and mutated $BRCA2_{1-250}$, established the stable $DLD1^{-/-}$ cell lines, performed kinase assays, pull-down assays, western blots, time-lapse microscopy experiments, mitotic index measurements by FACS and clonogenic survival assays as well as the statistical analysis for these experiments. M.J. performed the NMR experiments assisted by S. M., F.T. and S.Z.J.; S.M. performed the ITC experiments and purified $PLK1_{PBD}$; C.M. performed IF and image acquisition of metaphase plate alignment and chromosome segregation; V.B. assisted establishing stable clones and performing clonogenic survival assays; A.M. cloned and produced PLK1 from insect cells; A.C., A.E. and S.Z.J. designed the experiments; A.C. and S.Z.J. supervised the work; A.C. wrote the paper with important contributions from all authors.

Acknowledgments

We thank members of the AC lab for fruitful comments on the manuscript and Juan S. Martinez for construct $BRCA2_{1-250}$. We acknowledge the Cell and Tissue Imaging Facility of the Institut Curie (PICT), a member of the France BioImaging National Infrastructure (ANR-10-INBS-04) and the French Infrastructure for Integrated Structural Biology (https://www.structuralbiology.eu/networks/frisbi, (ANR-10-INSB-05-01).

This work was supported by the ATIP-AVENIR CNRS/INSERM Young Investigator grant 201201, EC-Marie Curie Career Integration grant CIG293444 to A.C. and Institut National du Cancer INCa-DGOS_8706 to A.C. and S.Z.J.; A.E. was supported by the Swedish Society for Medical Research.

The authors declare no conflict of interest.

Correspondence and requests for materials should be addressed to A.C.

References

1. Moynahan, M. E., Pierce, A. J. & Jasin, M. BRCA2 is required for homology-directed repair of chromosomal breaks. *Molecular Cell* **7,** 263–272 (2001).
2. Jensen, R. B., Carreira, A. & Kowalczykowski, S. C. Purified human BRCA2 stimulates RAD51-mediated recombination. *Nature* **467,** 678–683 (2010).
3. Saleh-Gohari, N. & Helleday, T. Conservative homologous recombination preferentially repairs DNA double-strand breaks in the S phase of the cell cycle in human cells. *Nucleic Acids Research* **32,** 3683–3688 (2004).
4. Fuks, F., Milner, J. & Kouzarides, T. BRCA2 associates with acetyltransferase activity when bound to P/CAF. *Oncogene* **17,** 2531–2534 (1998).
5. Futamura, M. *et al.* Potential role of BRCA2 in a mitotic checkpoint after phosphorylation by hBUBR1. *Cancer Res* **60,** 1531–1535 (2000).
6. Choi, E. *et al.* BRCA2 fine-tunes the spindle assembly checkpoint through reinforcement of BubR1 acetylation. *Developmental Cell* **22,** 295–308 (2012).
7. Mondal, G. *et al.* BRCA2 localization to the midbody by filamin A regulates cep55 signaling and completion of cytokinesis. *Developmental Cell* **23,** 137–152 (2012).
8. Daniels, M. J., Wang, Y., Lee, M. & Venkitaraman, A. R. Abnormal cytokinesis in cells deficient in the breast cancer susceptibility protein BRCA2. *Science* **306,** 876–879 (2004).
9. Takaoka, M., Saito, H., Takenaka, K., Miki, Y. & Nakanishi, A. BRCA2 phosphorylated by PLK1 moves to the midbody to regulate cytokinesis mediated by nonmuscle myosin IIC. *Cancer Res* **74,** 1518–1528 (2014).
10. Lin, H.-R., Ting, N. S. Y., Qin, J. & Lee, W.-H. M phase-specific phosphorylation of BRCA2 by Polo-like kinase 1 correlates with the dissociation of the BRCA2-P/CAF complex. *J Biol Chem* **278,** 35979–35987 (2003).
11. Lee, M., Daniels, M. J. & Venkitaraman, A. R. Phosphorylation of BRCA2 by the Polo-like kinase Plk1 is regulated by DNA damage and mitotic progression. *Oncogene* **23,** 865–872 (2004).
12. Zitouni, S., Nabais, C., Jana, S. C., Guerrero, A. & Bettencourt-Dias, M. Polo-like kinases: structural variations lead to multiple functions. *Nat Rev Mol Cell Biol* **15,** 433–452 (2014).

13. Barr, F. A., Silljé, H. H. W. & Nigg, E. A. Polo-like kinases and the orchestration of cell division. *Nat Rev Mol Cell Biol* **5,** 429–440 (2004).
14. Suijkerbuijk, S. J. E., Vleugel, M., Teixeira, A. & Kops, G. J. P. L. Integration of kinase and phosphatase activities by BUBR1 ensures formation of stable kinetochore-microtubule attachments. *Developmental Cell* **23,** 745–755 (2012).
15. Elowe, S., Hümmer, S., Uldschmid, A., Li, X. & Nigg, E. A. Tension-sensitive Plk1 phosphorylation on BubR1 regulates the stability of kinetochore microtubule interactions. *Genes Dev* **21,** 2205–2219 (2007).
16. Elowe, S. *et al.* Uncoupling of the spindle-checkpoint and chromosome-congression functions of BubR1. *J Cell Sci* **123,** 84–94 (2010).
17. Zhang, G., Mendez, B. L., Sedgwick, G. G. & Nilsson, J. Two functionally distinct kinetochore pools of BubR1 ensure accurate chromosome segregation. *Nature Communications* **7,** 12256 (2016).
18. Elia, A. E. H., Cantley, L. C. & Yaffe, M. B. Proteomic screen finds pSer/pThr-binding domain localizing Plk1 to mitotic substrates. *Science* **299,** 1228–1231 (2003).
19. Elia, A. E. H. *et al.* The molecular basis for phosphodependent substrate targeting and regulation of Plks by the Polo-box domain. *Cell* **115,** 83–95 (2003).
20. Neef, R. *et al.* Phosphorylation of mitotic kinesin-like protein 2 by polo-like kinase 1 is required for cytokinesis. *J Cell Biol* **162,** 863–875 (2003).
21. Kang, Y. H. *et al.* Self-regulated Plk1 recruitment to kinetochores by the Plk1-PBIP1 interaction is critical for proper chromosome segregation. *Mol. Cell* **24,** 409–422 (2006).
22. Szabo, C., Masiello, A., Ryan, J. F. & Brody, L. C. The breast cancer information core: database design, structure, and scope. *Hum. Mutat.* **16,** 123–131 (2000).
23. Béroud, C. *et al.* BRCA Share: A Collection of Clinical BRCA Gene Variants. *Hum. Mutat.* **37,** 1318–1328 (2016).
24. Hucl, T. *et al.* A syngeneic variance library for functional annotation of human variation: application to BRCA2. *Cancer Res* **68,** 5023–5030 (2008).
25. Giet, R. & Glover, D. M. Drosophila Aurora B Kinase Is Required for Histone H3 Phosphorylation and Condensin Recruitment during Chromosome Condensation and to Organize the Central Spindle during Cytokinesis. *J Cell Biol* **152,** 669–682 (2001).
26. Huang, H. *et al.* Phosphorylation sites in BubR1 that regulate kinetochore attachment, tension, and mitotic exit. *The Journal of Cell Biology* **183,** 667–680 (2008).
27. Yata, K. *et al.* BRCA2 coordinates the activities of cell-cycle kinases to promote genome stability. *CellReports* **7,** 1547–1559 (2014).
28. Yaffe, M. B. Structure and function of Polo-like kinases. *Oncogene* **24,** 248–259 (2005).
29. Park, I. *et al.* HDAC2/3 binding and deacetylation of BubR1 initiates spindle assembly checkpoint silencing. *FEBS J* (2017). doi:10.1111/febs.14286

Figure legends

Figure 1. BRCA2 VUS alter PLK1 phosphorylation of $BRCA2_{1-250}$

(a) PLK1 *in vitro* kinase assay with $BRCA2_{1-250}$. 7.5% SDS-PAGE showing the input of purified 2xMBP-$BRCA2_{1-250}$ WT and mutated proteins (0.5 μg) used in the reaction, as indicated. **(b)** The polypeptides encompassing $BRCA2_{1-250}$ WT or S193A, M192T, S196N, T200K, S206C, T207A mutations were incubated with recombinant PLK1 in the presence of γ^{32}P-ATP. The samples were resolved on 7.5% SDS-PAGE and the ^{32}P-labeled products were detected by autoradiography. **(c)** Quantification of (b). Data in (c) are represented as mean ± SD from at least three independent experiments (WT (n=9), S193A (n=4), M192T (n=4), S196N (n=4), S206C (n=4), T200K (n=5), T207A (n=4)). One-way ANOVA test with Tukey's multiple comparisons test was used to calculate statistical significance of differences (the asterisks show differences compared to WT; ns $p > 0.05$, * $p \leq 0.05$, ** $p \leq 0.01$, *** $p \leq 0.001$).

Figure 2. PLK1 phosphorylates T207 in $BRCA2_{190-283}$

Phosphorylation kinetics of $BRCA2_{190-283}$ as observed by NMR. **(a)** Superposition of the ^{1}H-^{15}N HSQC spectra recorded as a function of the phosphorylation time: from black (before phosphorylation) to red (after 24h with PLK1). PLK1 (1.1 μM) was incubated with ^{15}N labelled $BRCA2_{190-283}$ (200 μM) at 30°C and 200 μl were taken for each time point. Right panel: Zoom on the region containing the NMR signals of the phosphorylated residues. NMR peaks are labelled to indicate the corresponding residue following the timing colour code indicated in the left arrow (dark blue label: peaks appearing before 4 h; green label: peaks appearing before 5 h; red label: peaks observed only at 24 h). pT219 and pT226 give rise to several peaks (marked as (a), (b), (c)) as a function of the phosphorylation state of the surrounding residues. **(b)** Phosphorylation kinetics of S193 (red), T207 (black), T219 (blue) and T226

(grey). In the case of T226, the phosphorylation percentage corresponds to the sum of the intensities of peaks pT226(a), pT226(b) and pT226(c), which reflects the existence of different environments for phosphorylated T226 due to further phosphorylation of neighbouring T219 and S231. The multiplicity of the peaks corresponding to phosphorylated T226 at 24h hindered a proper measurement of this time point.

Figure 3. BRCA2 VUS alter PLK1 phosphorylation of BRCA2$_{190-283}$

(a) Superposition of the ^{1}H-^{15}N HSQC spectra recorded on VUS T207A as a function of the phosphorylation time: from black (before phosphorylation) to red (after 24h incubation with PLK1). The conditions are the same as in Figure 2a. A zoom on the region containing the NMR signals of the phosphorylated residues is shown. **(b)** Phosphorylation kinetics of T207 (black), S193 (red), T226 (grey) and T219 (blue), in WT (filled circles) versus T207A mutated BRCA2$_{190-283}$ (empty circles). **(c)** Superposition of the ^{1}H-^{15}N HSQC spectra recorded on variant T200K as a function of the phosphorylation time. **(d)** Phosphorylation kinetics of T207 (black), S193 (red), T226 (grey) and T219 (blue), in WT (filled circles) versus T200K mutated BRCA2$_{190-283}$ (empty circles).

Figure 4. BRCA2 variants showing reduced phosphorylation by PLK1 impair PLK1 binding

(a) 2xMBP-BRCA2$_{1-250}$ expressing the WT, the VUS (M192T, S196N, T200K, S206C and T207A) or the mutant S193A were expressed in U2OS cells by transient transfection for 30h before the cells were treated with nocodazole for 14h. Mitotic cells were lysed and immunoprecipitation was performed against the MBP tag using

amylose beads. Complexes were resolved on 4-15% SDS-PAGE followed by western blotting using anti-PLK1 and anti-MBP antibodies. **(b, c, d)** Isothermal Titration Calorimetry (ITC) thermograms showing binding of $PLK1_{PBD}$ to a 17 aa BRCA2 peptide containing **(b)** pT207, **(c)** T207, **(d)** A207, **(e)** C206pT207.

Figure 5. BRCA2 variants S206C and T207A delay mitosis and alter SAC activity

(a) Top: Scheme of the double thymidine block procedure used to synchronize $DLD1^{-/-}$ stable clones for live-cell imaging of cells progressing through mitosis. Bottom: Frequency distribution of the time cells spend in mitosis from anaphase onset to daughter cell separation monitored by time-lapse microscopy. ($DLD1^{+/+}$ (n=3), $DLD1^{-/-}$ (n=4), WT C1 (n=6), S206C A7 and A9 (n=3), T207A B1 and E4 (n=3)). **(b)** Representative still images of the live-cell imaging performed in Figure 5a at different time points. The time in each image indicates the min after mitotic onset. Scale bar represents 10 μm. **(c)** SAC activity was measured by flow cytometry analysis of p-histone 3 expression in $DLD1^{-/-}$ stable clones after treatment with nocodazole for 14h ($DLD1^{+/+}$ (n=3), $DLD1^{-/-}$ (n=7), WT C1 (n=7), S206C A7 (n=6) and A9 (n=4), T207A B1 (n=5) and E4 (n=5).

Statistical significance of the differences in (a) and (b) was calculated with two-way ANOVA test with Tukey's multiple comparisons test (the asterisks show differences compared to WT; ns $p > 0.05$, * $p \leq 0.05$, ** $p \leq 0.01$, *** $p \leq 0.001$, **** $p \leq 0.0001$).

Figure 6. Cells expressing BRCA2 variants that alter PLK1 phosphorylation display reduced protein levels of phosphorylated BUBR1 and misaligned chromosomes

(a, b) Western blots showing the expression levels of endogenous BUBR1 and (a) pT680-BUBR1 or (b) pS676-BUBR1 in nocodazole treated DLD1$^{-/-}$ stable clones expressing EGFPMBP-BRCA2 WT or VUS as indicated. StainFree images of the 4-15% SDS-PAGE gel before transfer were used as loading control (cropped image is shown). **(c)** Top: Scheme of the double thymidine block procedure used to synchronize DLD1$^{-/-}$ stable clones for analysis of chromosome alignment. Bottom: Quantification of misaligned chromosomes outside the metaphase plate in BRCA2 WT versus T207 expressing DLD1$^{-/-}$ stable clones. **(d)** Representative images of the type of chromosome alignment observed in cells expressing BRCA2 WT or T207A variant quantified in (c), scale bar represents 10 μm. Statistical significance of the difference in (c) was calculated with two-way ANOVA test with Tukey's multiple comparisons test (the asterisks show differences compared to WT; ns $p > 0.05$, * $p \leq 0.05$, ** $p \leq 0.01$, *** $p \leq 0.001$, **** $p \leq 0.0001$). *n* in (c) indicates the number of cells counted in each cell clone from a total of 2-4 independent experiments.

Figure 7. BRCA2 VUS S206C and T207A show aberrant chromosome segregation but display normal sensitivity to MMC

(a) Quantification of cells with aberrant chromosomes segregation in DLD1$^{-/-}$ stable BRCA2-WT, S206C and T207 clones. **(b)** Representative images of the type of aberrant chromosome segregation observed in the DLD1$^{-/-}$ stable clones expressing WT or VUS BRCA2 quantified in (a). CREST antibody is used as marker of centromere; nuclei are revealed with DAPI staining. Scale bars represents 10 μm. **(c)** Quantification of the surviving fraction of DLD1$^{-/-}$ stable clones assessed by clonogenic survival upon exposure to MMC at concentrations: 0, 0.5, 1.0 and 2.5 μM.

Data are represented as mean ± SD: DLD1$^{+/+}$ (red) (n=3), DLD1$^{-/-}$ (gray) (n=5), WT C1 (black) (n=5), S206C A7 (blue) (n=2), T207A B1 (green) (n=4). **(d)** Crystal violet stained colonies of unchallenged cells from (c). **(e)** Co-immunoprecipitation of endogenous PLK1 after exposure to IR (6 Gy) in nocodazole treated U2OS cells expressing exogenous 2xMBP-BRCA2$_{1\text{-}250}$ (WT). StainFree image of the 7.5% SDS-PAGE (7.5%) gel before transfer were used as loading control (cropped image is shown). **(f)** Model for the role of PLK1 phosphorylation of BRCA2 in mitosis (see text for details). In panels 2, 2', 3 and 3' blue blobs represent chromosomes, red cylinders represent the centrioles and orange lanes represent the spindle microtubules.

Statistical significance of the difference in (a) was calculated with one-way ANOVA test with Tukey's multiple comparisons test (the asterisks show differences compared to WT; ns $p > 0.05$, * $p \leq 0.05$, ** $p \leq 0.01$, *** $p \leq 0.001$, **** $p \leq 0.0001$). *n* in (a) indicates the number of cells counted in each cell clone from a total of 2-4 independent experiments.

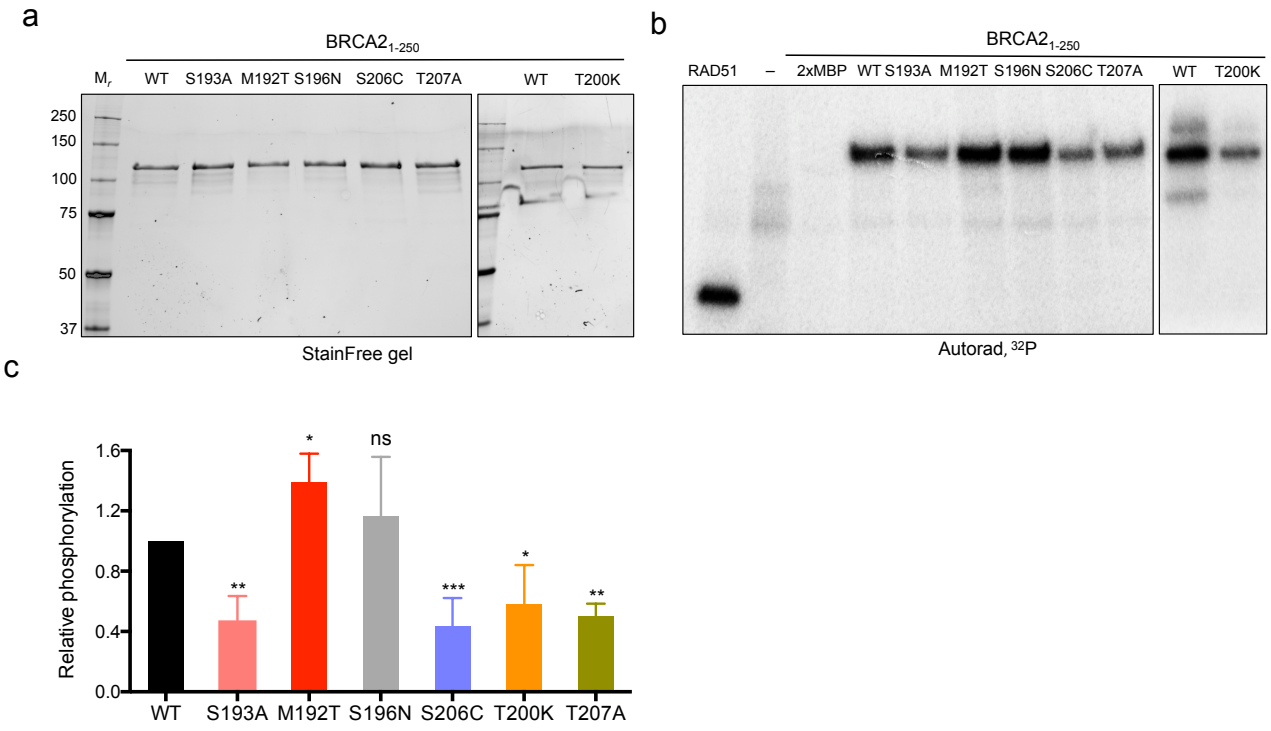

Figure 1

a

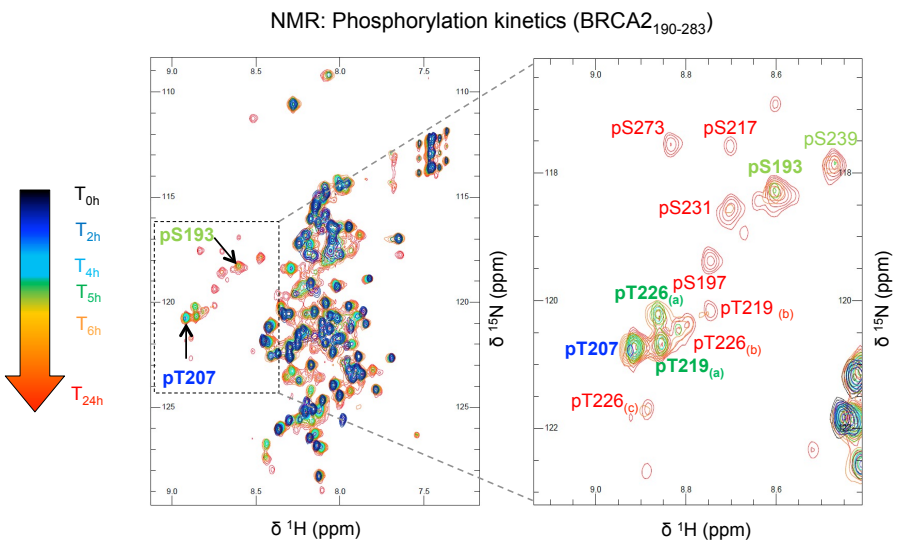
NMR: Phosphorylation kinetics (BRCA2190-283)
T0h
T2h
T4h
T5h
T6h
T24h
pS193
pT207
δ 15N (ppm)
δ 1H (ppm)
pS273
pS217
pS239
pS193
pS231
pS197
pT226(a)
pT219 (b)
pT207
pT226(b)
pT219(a)
pT226(c)

b

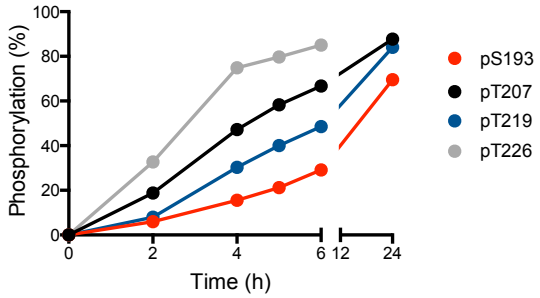
Phosphorylation (%)
100
80
60
40
20
0
0
2
4
6
12
24
Time (h)
pS193
pT207
pT219
pT226

Figure 2

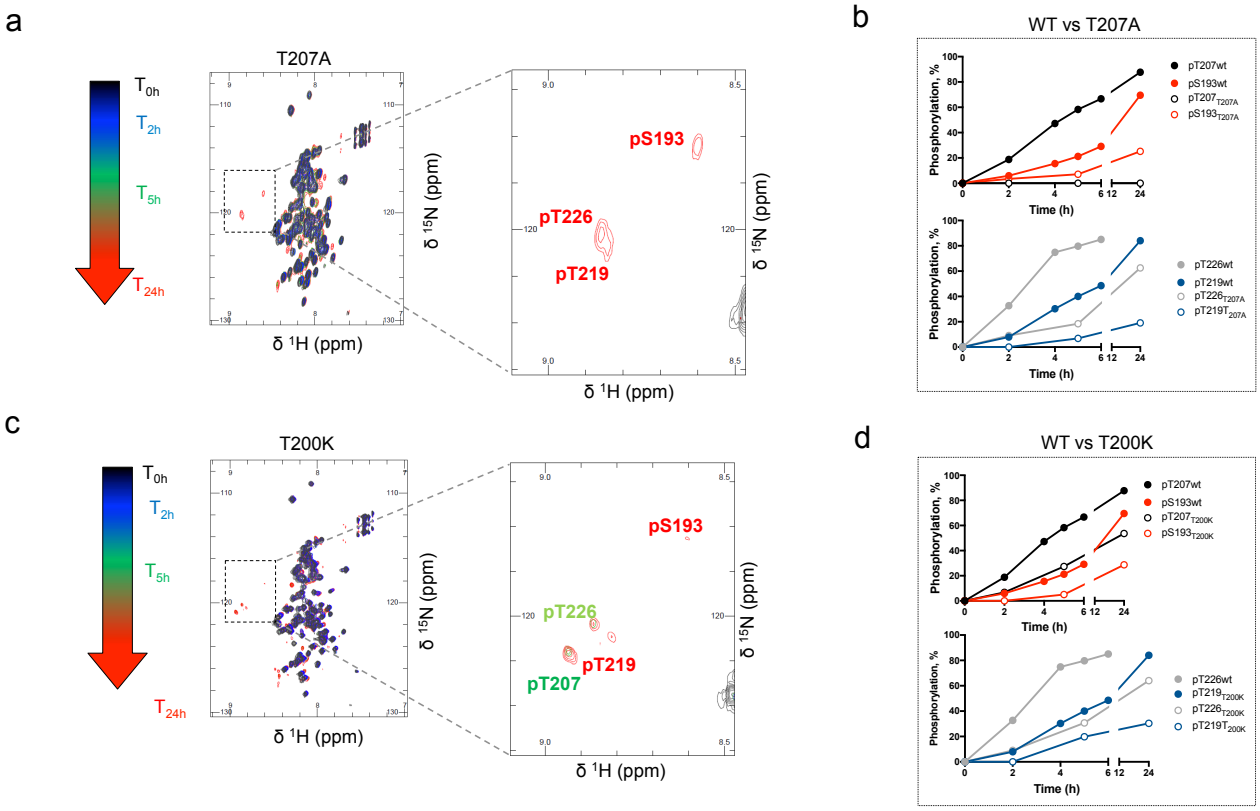
a
T207A
T0h
T2h
T5h
T24h
δ 1H (ppm)
δ 15N (ppm)
pS193
pT226
pT219
b
WT vs T207A
Phosphorylation, %
Time (h)
pT207wt
pS193wt
pT207T207A
pS193T207A
pT226wt
pT219wt
pT226T207A
pT219T207A
c
T200K
pS193
pT226
pT219
pT207
d
WT vs T200K
pT207wt
pS193wt
pT207T200K
pS193T200K
pT226wt
pT219T200K
pT226T200K
pT219T200K

Figure 3

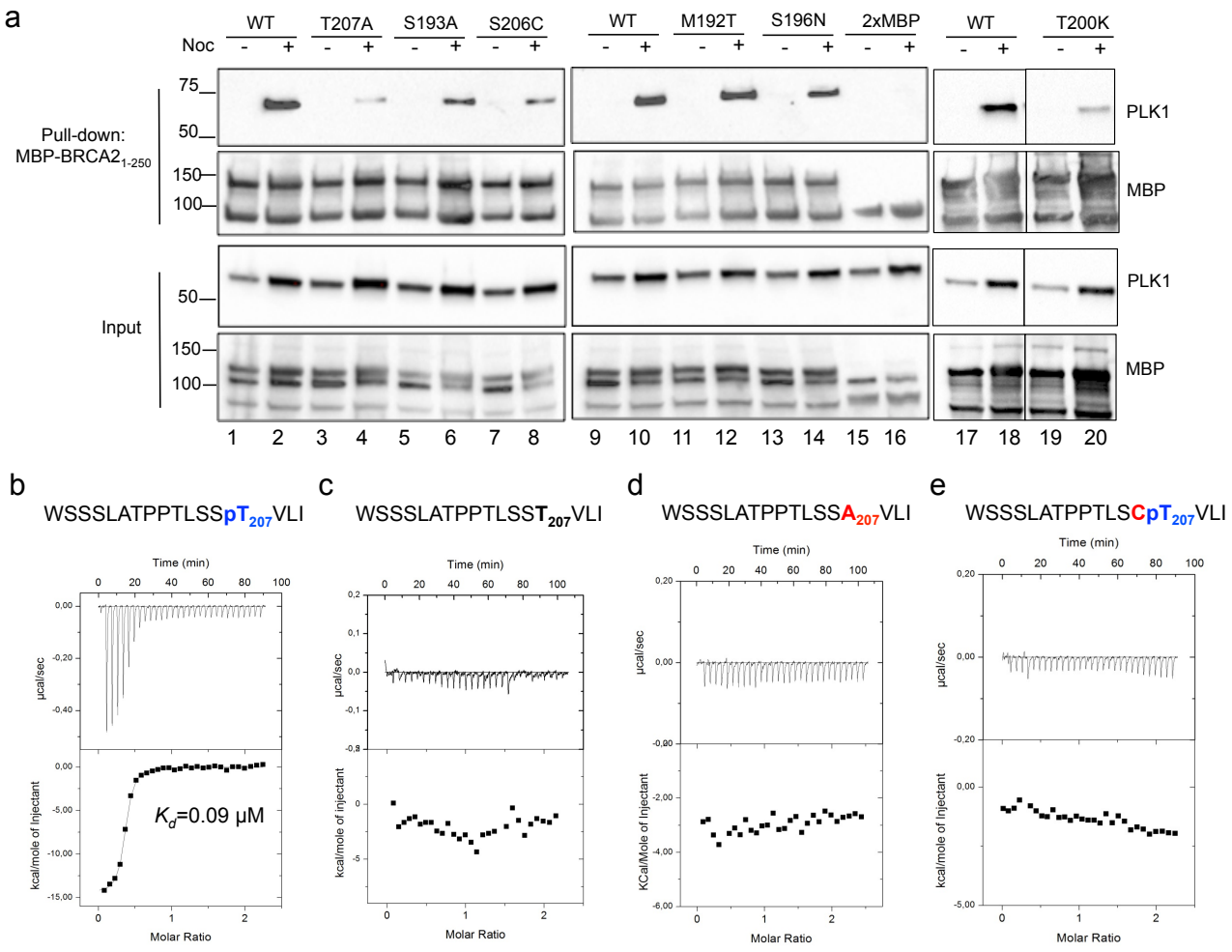
a
WT
T207A
S193A
S206C
WT
M192T
S196N
2xMBP
WT
T200K
Noc
- + - + - + - + - + - + - + - + - + - +
75
50
150
100
Pull-down:
MBP-BRCA2 1-250
PLK1
MBP
50
150
100
Input
PLK1
MBP
1 2 3 4 5 6 7 8 9 10 11 12 13 14 15 16 17 18 19 20
b
WSSSLATPPTLSSpT207VLI
Time (min)
µcal/sec
kcal/mole of injectant
Kd=0.09 µM
Molar Ratio
c
WSSSLATPPTLSST207VLI
Time (min)
µcal/sec
kcal/mole of injectant
Molar Ratio
d
WSSSLATPPTLSSA207VLI
Time (min)
µcal/sec
KCal/Mole of Injectant
Molar Ratio
e
WSSSLATPPTLSCpT207VLI
Time (min)
µcal/sec
kcal/mole of injectant
Molar Ratio

Figure 4

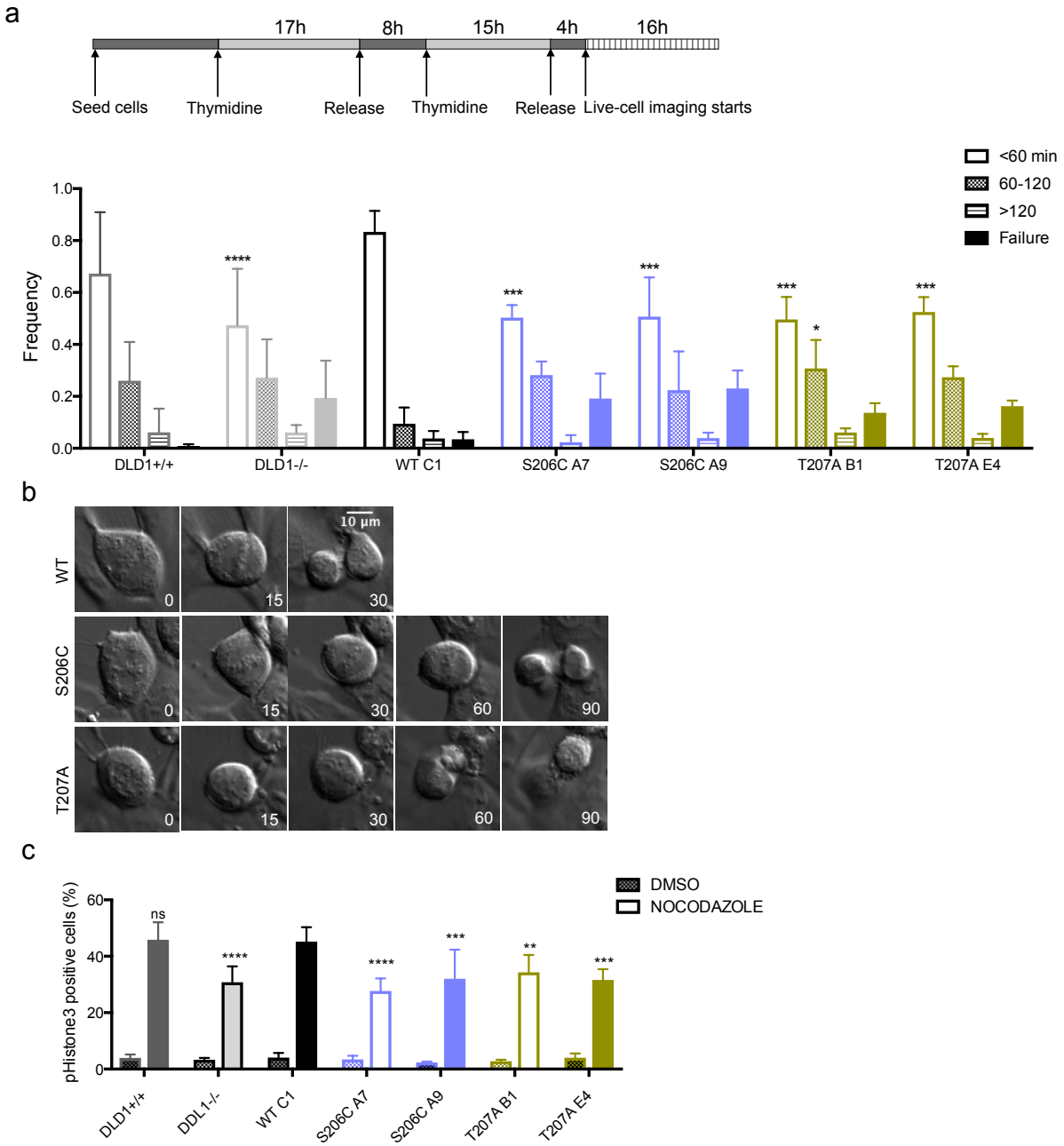
a
17h
8h
15h
4h
16h
Seed cells
Thymidine
Release
Thymidine
Release
Live-cell imaging starts
<60 min
60-120
>120
Failure
Frequency
1.0
0.8
0.6
0.4
0.2
0.0
****
***
***
***
*
***
DLD1+/+
DLD1-/-
WT C1
S206C A7
S206C A9
T207A B1
T207A E4
b
10 µm
WT
S206C
T207A
0
15
30
60
90
c
DMSO
NOCODAZOLE
pHistone3 positive cells (%)
60
40
20
0
ns
****
****
***
**
***
DLD1+/+
DDL1-/-
WT C1
S206C A7
S206C A9
T207A B1
T207A E4

Figure 5

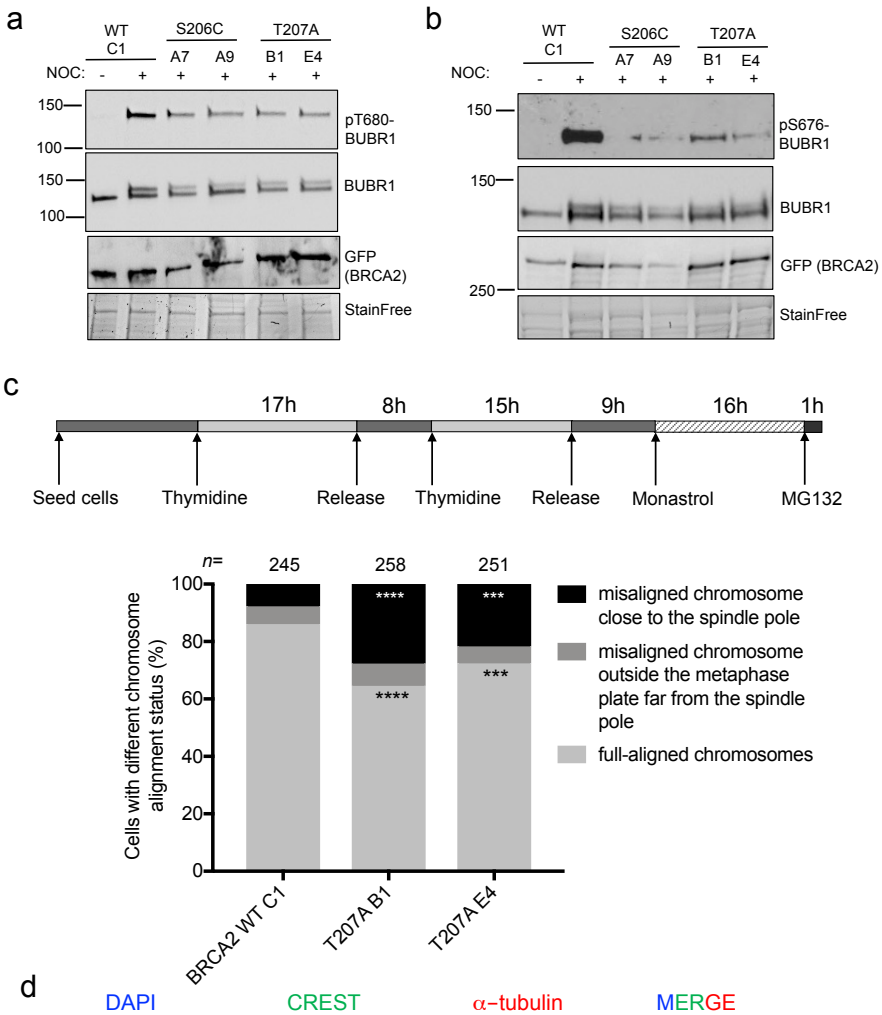
a
WT
C1
S206C
A7
A9
T207A
B1
E4
NOC:
150
100
pT680-
BUBR1
BUBR1
GFP
(BRCA2)
StainFree
b
pS676-
BUBR1
250
c
17h
8h
15h
9h
16h
1h
Seed cells
Thymidine
Release
Thymidine
Release
Monastrol
MG132
n=
245
258
251
Cells with different chromosome alignment status (%)
misaligned chromosome close to the spindle pole
misaligned chromosome outside the metaphase plate far from the spindle pole
full-aligned chromosomes
BRCA2 WT C1
T207A B1
T207A E4
d
DAPI
CREST
α-tubulin
MERGE
10 µm

Figure 6

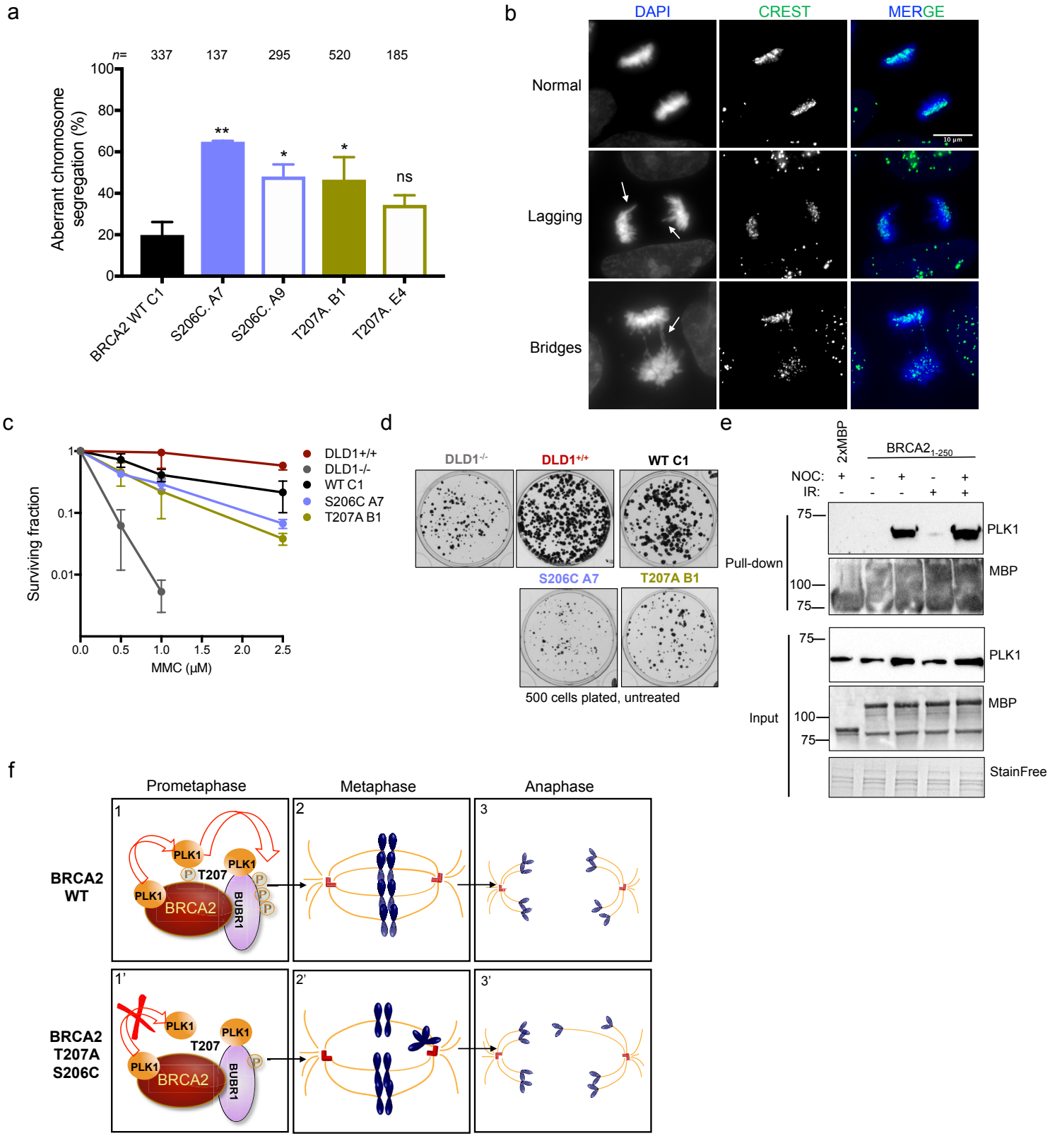
a
n= 337 137 295 520 185
Aberrant chromosome segregation (%)
100
80
60
40
20
0
**
*
*
ns
BRCA2 WT C1
S206C. A7
S206C. A9
T207A. B1
T207A. E4
b
DAPI
CREST
MERGE
Normal
Lagging
Bridges
10 µm
c
Surviving fraction
1
0.1
0.01
0.0 0.5 1.0 1.5 2.0 2.5
MMC (µM)
DLD1+/+
DLD1-/-
WT C1
S206C A7
T207A B1
d
DLD1-/-
DLD1+/+
WT C1
S206C A7
T207A B1
500 cells plated, untreated
e
2xMBP
BRCA2 1-250
NOC: + - + - +
IR: - - - + +
Pull-down
75
PLK1
MBP
100
75
Input
75
PLK1
MBP
100
75
StainFree
f
Prometaphase
Metaphase
Anaphase
BRCA2 WT
1
2
3
PLK1
T207
BRCA2
BUBR1
BRCA2 T207A S206C
1'
2'
3'

Figure 7

METHODS

Cell lines, cell culture and synchronisations

The human cell lines HEK293T and U2OS cells (kind gift from Dr. Mounira Amor-Gueret) were cultured in DMEM (Eurobio Abcys, Courtaboeuf, France) media containing 25 mM sodium bicarbonate and 2 mM L-Glutamine supplemented with 10% heat inactive FCS (EuroBio Abcys). The BRCA2 deficient colorectal adenocarcinoma cell line DLD1 BRCA2$^{-/-}$ (hereafter DLD$^{-/-}$) (Hucl, T. et al 2008) (HD 105-007) and the parental cell line DLD1 (HD-PAR-008) was purchased from Horizon Discovery (Cambridge, England). The cells were cultured in RPMI media containing 25 mM sodium bicarbonate and 2 mM L-Glutamine (EuroBio Abcys) supplemented with 10% heat inactive FCS (EuroBio Abcys). The DLD1 BRCA2$^{-/-}$ cells were maintained in growth media containing 0.1 mg/ml hygromycin B (Thermo Fisher Scientific). The stable cell lines of DLD1$^{-/-}$ expressing BRCA2 WT or variants of interest generated in this study were cultured in growth media containing 0.1 mg/ml hygromycin B and 1 mg/ml G418 (Sigma-Aldrich). All cells were cultured at 37°C with 5% CO_2 in a humidified incubator and all cell lines used in this study have been regularly tested negatively for mycoplasma contamination.

For synchronization of cells in mitosis, nocodazole (100-300 ng/ml, Sigma-Aldrich) was added to the growth media and the cells were cultured for 14h before harvesting.

For synchronisation by double thymidine block, the cells were treated with thymidine (2.5 mM, Sigma-Aldrich) for 17h, released for 8h followed by a second thymidine (2.5 mM) treatment for 15h.

Plasmids

2XMBP-, 2XMBP-BRCA2$_{1-250}$ and EGFP-MBP-BRCA2 subcloning in phCMV1 expression vector were generated as described (Martinez et al., 2016; Nicolai et al., 2016). In the case of 2XMBP and 2XMBP-BRCA2$_{1-250}$, a tandem of 2 nuclear localization signals from RAD51 sequence was added downstream the MBP-tag. Point mutations (M192T, S193A, S196N, S206C, T200K and T207A) were introduced in the 2xMBP-BRCA2$_{1-250}$, EGFP-MBP-BRCA2 vector using QuikChange II and QuikChange XL site-directed mutagenesis kit (Agilent Technologies), respectively (see Supplementary information, Table S1 for primer sequences).
For expression of BRCA2$_{190-283}$ in bacteria, the human BRCA2$_{192-283}$ was amplified by PCR using full length BRCA2 as template (phCMV1-BRCA2). The PCR product was purified and digested with *BamH1* and *SalI* and cloned into in the pGEX-6P-1 vector (GE Healthcare) to generate GST-BRCA2$_{192-283}$, which was then modified by site-directed mutagenesis to generate GST-BRCA2$_{190-283}$ (see Supplementary information, Table S3 for primer sequences). The point mutations (M192T, T200K and T207A) were introduced in the same way as for 2xMBP-BRCA2$_{1-250}$ and the EGFP-MBP-BRCA2. The introduction of the point mutations was verified by sequencing (see Supplementary information, Table S2 for sequencing primers).

The *PLK1* cDNA (Addgene pTK24) was cloned into the pFast-Bac HT vector using Gibson assembly (NEB) (see Supplementary information, Table S4 for primer sequences). The Polo-like binding domain (PBD) of PLK1 (amino acid 326 to amino acid 603) was amplified from the pTK24 plasmid (Addgene) and cloned into a pT7-His6-SUMO expression vector using Gibson assembly (NEB) (see Supplementary information, Table S5 for primer sequences).

Expression and purification of 2xMBP-BRCA2$_{1-250}$

The 2xMBP-BRCA2$_{1-250}$ was purified as earlier described (von Nicolai *et al.,* 2016). Briefly, ten 150 mm plates of HEK293T were transient transfected with the 2xMBP-BRCA2$_{1-250}$ using TurboFect (Thermo Fisher Scientific). The cells were harvested 30 h post transfection, lysed in lysis buffer H (50 mM HEPES (pH 7.5), 250 mM NaCl, 1% NP-40, 5 mM EDTA, 1 mM DTT, 1 mM PMSF and EDTA-free Protease Inhibitor Cocktail (Roche)) and incubated with amylose resin (NEB) for 3h at 4°C. The 2xMBP-BRCA2$_{1-250}$ was eluted with 10 mM maltose. The eluate was further purified with Bio-Rex 70 cation-exchange resin (Bio-Rad) by NaCl step elution. The size and purity of the final fractions were analysed by SDS-PAGE and western blotting using anti-MBP antibody. The 2xMBP-BRCA2$_{1-250}$ fragments containing the BRCA2 variants (M192T, S193A, S196N, S206C, T200K and T207A) were purified in the same way as WT 2xMBP-BRCA2$_{1-250}$.

Expression and purification of BRCA2$_{190-283}$ for NMR

Recombinant ^{15}N-labelled (WT, T200K, T207A,) and ^{15}N/^{13}C-labelled (WT, T207A) BRCA2$_{190-283}$ were produced by transforming *Escherichia coli* BL21 (DE3) Star cells (Protein Expression and Purification Core Facility, Institut Curie) with the pGEX-6P-1 vector containing human BRCA2$_{190-283}$ (WT and the variants) following standard heat-shock transformation protocols. Cells were grown in a M9 medium containing 0.5 g/l $^{15}NH_4Cl$ and 2 g/l ^{13}C-glucose when ^{13}C labelling was needed. The bacterial culture was induced with 1 mM IPTG at an OD_{600} of 0.8, and it was further incubated for 3 h at 37°C. Harvested cells were resuspended in buffer A (50 mM Tris-HCl pH 7.5, 150 mM NaCl, 2 mM DTT, 1 mM EDTA) with 5 % glycerol, 10% Triton X-100, 1 mM PMSF and protease inhibitors cocktail (Roche) and disrupted by sonication. Clarified

cell lysate was loaded on Glutathione (GSH) Sepharose beads (GE Healthcare) equilibrated with buffer A. After 2 h of incubation at room temperature, beads were washed with buffer A and eluted with buffer A containing 20 mM reduced glutathione. The tag was cleaved by the precision protease during an overnight dialysis at 4°C against buffer B (50 mM HEPES pH 7.0, 1 mM EDTA) with 2 mM DTT and 150 mM NaCl. The cleaved GST-tag was removed by heating the sample for 15 min at 95°C and spun it down for 10 min at 16,000 x *g*. Sample concentration was calculated using its estimated molecular extinction coefficient of 10,363 M^{-1} cm^{-1} at 280 nm. The protein sample was characterized for folding using NMR HSQC spectra, before and after the heating at 95°C. $BRCA2_{190-283}$ was dialyzed overnight at 4°C against buffer B with 2 mM DTT.

Expression and purification of PLK1

The recombinant 6his-PLK was produced in sf9 insect cells by infection for 48h (28°C, 110 rpm shaking) with the recombinant baculovirus (PLK1-pFast-Bac HT vector). Infected cells were collected by centrifugation (1300 rpm, 10 min, 4°C), washed with 1xPBS, resuspended in lysis buffer (1xPBS, 350 mM NaCl, 1% Triton X-100, 10% glycerol, EDTA-free Protease Inhibitor Cocktail (Roche), 30 mM imidazole). After 1h rotation at 4°C the lysate was centrifuged (25000 rpm, 1h, 4°C) and the supernatant was collected, filtered (0.4 µm) and loaded immediately onto a Ni-NTA column (Macherey Nagel) equilibrated with Buffer A1 (1xPBS with 350 mM NaCl, 10% glycerol and 30 mM imidazole, the column was washed with buffer A2 (1xPBS with 10% glycerol) and the protein was eluted with Buffer B1 (1x PBS with 10% glycerol and 250 mM imidazole). The eluted protein was diluted to 50 mM NaCl with Buffer A before being loaded onto a cationic exchange Capto S column (GE

Healthcare) equilibrated with Buffer A1cex (50 mM HEPES (pH 7.4), 50 mM NaCl and 10% glycerol), the column was washed with Buffer A1cex before elution with Buffer B1cex (50 mM HEPES (pH 7.4), 2M NaCl and 10% glycerol). The quality of the purified protein was analysed by SDS-PAGE and the proteins concentration was determined using Bradford protocol with BSA as standard. The purest fractions were pooled and dialyzed against storage buffer (50 mM Tris-HCl (pH7.5), 150 mM NaCl, 0.25 mM DTT, 0.1 mM EDTA, 0.1 mM EGTA, 0.1 mM PMSF and 25% Glycerol) and stored in -80°C. The purified protein can be seen in Figure S7A.

Expression and purification of PLK1$_{PBD}$

The pT7-6His-Sumo-PLK1 PBD (326-603) plasmid was expressed in Tuner pLacI pRare cells (Protein Expression and Purification Core Facility, Institut Curie), 2L of TB medium with Kanamycin and Chloramphenicol antibiotics were inoculated with cells from the pre-culture. The cells were grown at 37°C until an OD_{600} of ~ 0.85. The temperature was decreased to 20°C and the expression was induced by 1mM IPTG overnight. The cells were harvested by 15 min of centrifugation at 4690 *x g*, at 4 °C. The cell pellets were suspended in 80 ml of 1 x PBS, pH 7.4, 150 mM NaCl, 10% glycerol, EDTA-free Protease Inhibitor Cocktail (Roche), 5 mM β-mercapto-ethanol (β-ME). The suspension was treated with benzonase nuclease and $MgCl_2$ at 1 mM final concentration for 20 min at 4°C. The suspension was lysed by disintegration at 2 kbar (Cell distruptor T75, Cell D) followed by centrifugation at 43000 *x g*, for 45 min, at 4 °C. The supernatant was loaded at 1 ml/min on a His-Trap FF-crude 5 mL column (GE Healthcare) equilibrated with PBS buffer, pH 7.4, 150 mM NaCl, 10% glycerol, 5 mM β-ME (A) and 20 mM imidazole. The proteins were eluted in a linear gradient from 0 to 100 % with the same buffer (A) containing 200 mM imidazole, over

10 column volumes (CV). The purest fractions were pooled and dialyzed (8 kDa cut-off) against 20 mM Tris-HCl buffer, pH 8.0, 100 mM NaCl, 0.5 mM EDTA, 5 mM β-ME, 10% glycerol at 4 °C. 6xHis-SUMO Protease (Protein Expression and Purification Core Facility, Institut Curie) was added at 1/100 (w/w) and incubated overnight at 4 °C to cleave the 6His-SUMO tag. The cleaved PBD-PLK1 was purified using Ni-NTA agarose resin (Macherey Nagel), washed with the following buffer: 20 mM Tris-HCl pH 8.0, 100 mM NaCl, 0.5 mM EDTA, 5mM β-ME and 10 % glycerol. The sample was incubated with the resin for 1h at 4 °C and the flow-through was collected.

The sample was concentrated on an Amicon Ultra Centrifugal Filter Unit (10 kDa cut-off) and injected at 0.5 mLl/min on a Hi-Load 16/60 Superdex column (GE healthcare), equilibrated with 20 mM Tris-HCl buffer, pH 8.0, 100 mM NaCl, 0.5 mM EDTA, 5 mM β-ME. The protein concentration was estimated by spectrophotometric measurement of absorbance at 280 nm. The purified protein can be seen in Figure S7B.

***In vitro* PLK1 kinase assay**

0.5 µg purified 2xMBP-BRCA2$_{1-250}$ or 25 ng RAD51 protein, was phosphorylated by 0.1 µg recombinant active PLK1 (purchased from Abcam or purified from sf9 insect cells as detailed above, see Figure S6C to see the comparison of the kinase activity of both PLK1 preparations) in kinase buffer (25 mM HEPES, pH 7.6, 25 mM ß-glycerophosphate, 10 mM $MgCl_2$, 2 mM EDTA, 2mM EGTA, 1 mM DTT, 1 mM Na_3VO_4, 10 µM ATP and 1 µCi γ^{32}P-ATP (Perkin Elmer)) in a 25 µl total reaction volume. After 30 min incubation at 30°C the reaction was stopped by heating at 95°C for 5 min in SDS-PAGE sample loading buffer. The samples were resolved by 7.5 %

SDS-PAGE and ^{32}P-labelled bands were analysed with PhosphorImager (Amersham Bioscience) using ImageQuant^{TM} TL software (GE Healthcare Life Science). To control for the amount of substrate in the kinase reaction, before adding γ^{32}P-ATP, half of the reaction was loaded on a 7.5 % stain free SDS-PAGE gel (BioRad), the protein bands were visualized with ChemiDoc XRS+ System (BioRad) and quantified by Image Lab^{TM} 5.2.1 Software (BioRad). The relative phosphorylation of 2xMBP-BRCA2$_{1-250}$ was quantified as ^{32}P-labelled 2xMBP-BRCA2$_{1-250}$ (ImageQuant^{TM} TL software) divided by the intensity of the 2xMBP-BRCA2$_{1-250}$ band in the SDS-PAGE gel (Image Lab^{TM} 5.2.1 Software).

NMR spectroscopy

Most NMR experiments were carried out at 283 K on 600 and 700 MHz Bruker spectrometers. For NMR signal assignments, standard 3D triple resonance NMR experiments were recorded on BRCA2$_{190-283}$ WT and T207A. Analyses of these experiments provided backbone resonance assignment of the non-phosphorylated and phosphorylated forms of these BRCA2 fragments. To follow the PLK1 phosphorylation kinetics, ^{1}H-^{15}N HSQC were recorded at each time point. Data processing and analysis were carried out using Topspin and CcpNmr Analysis 2.4.2 software.

Analysis of phosphorylation assays followed by NMR

In the HSQC spectra, the intensity of peaks of each phosphorylated residue (pT207, pT226, pT219, pS193) as well as the intensity of peaks corresponding to their non-phosphorylated form was retrieved at each time point of the kinetics. In order to estimate the fraction of phosphorylation for each residue at each point, the function

$Intensity_{(phospho)} = f[Intensity_{(non\text{-}phospho)}]$ was drawn for each residue, the trendline was extrapolated to determine the intensity corresponding to the 100% phosphorylated residue and then the percentage of phosphorylation could be calculated at each time point by dividing peak intensities corresponding to the phosphorylated residue by the calculated intensity at 100% phosphorylation. Peaks corresponding to residues closed to a phosphorylated residue (L209 and V211 for pT207; A227, K230, V229 and Y232 for pT226; F221, E218 and A216 for pT219; D191, S197 and S195 for pS193) and thus affected by this phosphorylation were also treated using the same protocol and they were used to obtain a final averaged curve of the evolution of the percentage of phosphorylation at positions 193, 207, 219 and 226 with time.

Isothermal Titration Calorimetry

ITC measurements were performed using a VP-ITC instrument (Malvern), at 293 K, with peptide and protein samples in 50 mM Tris-HCl buffer, pH 8.0 containing 150 mM NaCl and 5 mM β-mercaptoethanol. We used automatic injections of 8 or 10 µl. The titration data were analyzed using the program Origin 7.0 and fitted to a one-site binding model. To evaluate the heat of dilution, the control experiments were done with peptide or protein solutions injected into the buffer. The peptides used for the ITC experiments were synthesized by GeneCust (Ellange, LU) or Genscript (Piscataway, NY). All the peptides were acetylated and amidated at the N-terminal and C-terminal ends, respectively (see Supplementary information, Table S5 for primer sequences).

Generation of stable DLD1 clones

For generation of DLD1 cell lines stably expressing BRCA2 variants of interest, we transfected one 100 mm plate of DLD1 BRCA2$^{-/-}$ cells at 70% of confluence with 10 µg of EGFPMBP-BRCA2 plasmid using TurboFect (Thermo Fisher Scientific), 48h post-transfection the cells were serial diluted and cultured in media containing 1 mg/ml G418 (Sigma-Aldrich) for selection. Single cells were isolated and expanded. To verify and select the clones, cells were resuspended in cold lysis buffer H (50 mM HEPES (pH 7.5), 250 mM NaCl, 1% NP-40, 5 mM EDTA, 1 mM DTT, 1 mM PMSF and EDTA-free Protease Inhibitor Cocktail (Roche)), incubated on ice for 30 min, sonicated and centrifuged at 10,000 x *g* for 15 min, 100 µg total protein lysate was run on a 4-15% SDS-PAGE followed by immunoblotting using BRCA2 and GFP antibodies to detect GFP-MBP-BRCA2. Clones with similar expression levels were selected for functional studies.

The presence of the point mutations in the genome of the clones was confirmed by extraction of genomic DNA using Quick-DNA^{TM} Universal Kit (ZYMO Research) followed by amplification of the N-terminal of BRCA2 (aa 1-267) by PCR using a forward primers that binds to the end of MBP and a reveres primer that binds to amino acid 267 in BRCA2, the presence of the point mutations was confirmed by sequencing of the PCR product (see Supplementary information, Table S7 for primer sequences).

Cell extracts, immunoprecipitation and western blotting

For the interaction between BRCA2$_{1-250}$ and endogenous PLK1, U2OS cells were transfected with 2xMBP-BRCA2$_{1-250}$ construct (WT, M192T, S193A, S196N, S206C, T200K and T207A) using TurboFect (Thermo Fisher Scientific), 30 h post-transfection cells were synchronized by nocodazole (300 ng/ml), harvested and lysed

in extraction buffer A (20 mM HEPES (pH 7.5), 150 mM NaCl, 0.1% NP40, 2 mM EGTA, 1.5 mM $MgCl_2$, 50 mM NaF, 10 % glycerol, 1 mM Na_3VO_4, 20 mM ß-glycerophosphate, 1 mM DTT and EDTA-free Protease Inhibitor Cocktail (Roche)). After centrifugation at 18,000 x *g* for 15 min, the supernatant was incubated with amylose resin (NEB) for 1.5h at 4°C. The beads were washed five times in extraction buffer before elution with 10 mM maltose. Bound proteins were separated by SDS-PAGE and analysed by western blotting. Where PLK1 inhibitor was used, the cells were synchronized in mitosis by nocodazole (14h) followed by 2h treatment with either 50 nM Bi2536 (Selleckchem) or 50 uM BTO-1 (Sigma-Aldrich) before harvesting. The cells were lysed in extraction buffer, pre-cleared by centrifugation and total protein lysate was separated by SDS-PAGE and analysed by western blotting. For the pull-down experiments after exposure to IR, U2OS cells were transient transfected with 2xMBP-$BRCA2_{1-250}$ WT construct, and exposed to IR (6 Gy) using a ^{137}Cs source after 14h treatment with nocodazole. The cells were immediately harvested and lysed (as described above) after irradiation.
For BUBR1 and pBUBR1 levels in mitosis, nocodazole (100 ng/ml) treated DLD1 clones were lysed in extraction buffer A, pre-cleared by centrifugation and total protein lysate was separated by SDS-PAGE and analysed by western blotting. Where PLK1 inhibitor was used, the cells were synchronized in mitosis by nocodazole (100 ng/ml) for 14h followed by 2h treatment with either 50 nM Bi2536 (Selleckchem) or 50 uM BTO-1 (Sigma-Aldrich) before harvesting.

Proteins were detected by western blotting using following primary antibodies: mouse anti-MBP (1:5000, R29, Cat. #MA5-14122, Thermo Fisher Scientific), mouse anti-BRCA2 (1:1000, OP95, EMD Millipore), rabbit anti-GFP (1:5000, Protein

Expression and Purification Core Facility, Institut Curie), mouse anti-PLK1 (1:5000, clone 35-206, Cat. #05-844, EMD Millipore, 1:5000), mouse anti-BUBR1 (1:1000, Cat. #612502, BD Transduction laboratories), rabbit anti-pT680-BUBR1 (1:1000, EPR 19958, Cat. #ab200061) and rabbit anti-pS676-BUBR1 (1:1000, R193, kind gift from Dr. Erich A Nigg). Horseradish peroxidase (HRP) conjugated 2nd antibodies used: mouse-IgGκ BP-HRP (IB: 1:10 000, Cat. #sc-516102, Santa Cruz), goat anti-rabbit IgG-HRP (IB: 1:5000, Cat. #sc-2054, Santa Cruz), goat anti-mouse IgG-HRP (1:10 000, Cat.# 115-035-003, Interchim), goat anti-rabbit IgG-HRP (1:10 000, Interchim, Cat.# 111-035-003),

Phosphatase treatment

DLD1$^{-/-}$ cells stably expressing EGFP-MBP-BRCA2 WT were synchronized in mitosis by nocodazole (14h), harvested, lysed in extraction buffer A and pre-cleared by centrifugation. Increased amount (0-20U) of FastAP Thermosensitive Alkaline Phosphatase (Thermo Fisher Scientific Cat. #EF0654) was added to 15 ug of total protein lysate in FastAP Buffer in a total reaction volume of 60 ul. After 1h incubation at 37°C the reaction was stopped by heating at 95°C for 5 min in SDS-PAGE sample loading buffer, 30 ul of the reaction was loaded on a 4-15 % SDS-PAGE gel, the gel was transferred onto nitrocellulose membrane and the levels of pT680-BUBR1 was analysed by western blotting.

Cell survival assay

For clonogenic survival assay, DLD1 cells stably expressing full-length GFPMBP-BRCA2 and the variants (S206C and T207A) were treated at 70% of confluence with Mitomycin C (Sigma-Aldrich) at concentrations: 0, 0.5, 1.0 and 2.5 μM. After 1 h drug

treatment the cells were serial diluted in normal growth media containing penicillin/streptomycin (Eurobio) and seeded in triplicates into 6-well plates. The media was changed every third day, after 10-12 days in culture the plates were stained with crystal violet, colonies were counted and the surviving fraction was determined for each drug concentration.

Cell cycle analysis and mitotic index

DLD1 cells stably expressing full-length GFPMBP-BRCA2 and the variants (S206C and T207A) were nocodazole (100 ng/ml, Sigma-Aldrich) or mock treated for 14h, trypsinized, washed in PBS and fixed in cold 70% ethanol at -20ºC overnight. The cells were washed twice in cold 1 x PBS before staining with rabbit anti-histone3 (phosphor-Ser10) antibody (1:200, Cat. #06-570, EMD Millipore) in staining buffer (1 x PBS, 3% FBS) for 1h in room temperature. The cells were then washed with 1 x PBS before staining for 30 min at room temperature with a chicken anti-rabbit Alexa-Fluor-647-conjugated antibody (1:250, Cat. #A-21443, Life Technologies). After one wash in 1 x PBS the cells were resuspended in 7-AAD (559925, BD Pharmingen) and diluted in staining buffer. The DNA content and p-Histone 3 staining were visualized with a FACSCanto and data were analysed with FlowJo software (Tree Star Inc.).

Immunofluorescence

DLD1 cells stably expressing full-length GFPMBP-BRCA2 and the variants (S206C and T207A) were seeded on coverslips in 6-well tissue culture plates and synchronized in mitosis. For analysis of chromosome alignment, the cells were synchronized by double thymidine block, released for 9h followed by 16h treatment

with monastrol (100 uM, Sigma-Aldrich) before being released for 1h in the presence of the proteasome inhibitor MG-132 (10 μM, Sigma-Aldrich). For chromosome segregation analysis, the cells were released from double thymidine block and cultured for 11h in normal growth media. The cells were fixed with 100% methanol for 15 min at -20ºC, washed once in PBS before permeabilization with PBS containing 0.1% Trition-X for 15 min at room temperature. Nonspecific epitopes were blocked with 4% BSA (Sigma-Aldrich) in PBS. The cells were washed in PBS and then incubated with primary antibody diluted in PBS containing 0.1% Tween-20 (PBS-T) and 5% BSA for 1h at room temperature. The coverslips were washed three times of 5 min in PBS-T before being incubated for 1h at room temperature with respective Alexa Fluor conjugated secondary antibody diluted in PBS-T with 5% BSA. After two more wash steps of 5 min each in PBS-T and one rinse in PBS the coverslips were mounted with DAPI (ProLong Diamond Antifade Mountant with DAPI, Thermo Fisher Scientific) on microscope slides.

Primary antibodies used for immunofluorescence analysis: human anti-CREST (1:100, Cat. #15-234-0001, Antibodies Online) and mouse anti-αtubulin (1:5000, GT114, Cat. #GTX628802, Euromedex). Alexa Fluor conjugated secondary antibodies used: goat anti-human Alexa-488 (1:1000, Cat. # A11013, Life Technologies), goat anti-mouse Alexa-594 (1:1000, Cat. #A21203, Life Technologies). Images were acquired in an upright Leica DM6000B widefield microscope equipped with a Leica Plan Apo 63x NA 1.4 oil immersion objective. The camera used is a Hamamatsu Flash 4.0 sCMOS controlled with MetaMorph2.1 software (Molecular Devices). For Figures 6d and 7b, 7 to 20 Z-stacks were taken at 0.5 μm intervals to generate a maximal intensity projection image using ImageJ.

Time-lapse video microscopy of mitotic cells

For phase-contrast video-microscopy DLD1 cells stably expressing full-length GFPMBP-BRCA2 and the variants (S206C and T207A) were seeded in 35 mm Ibidi µ-Dishes (Ibidi), synchronized by double thymidine block, released and cultured for 4h in normal growth media before the filming was started. The cells were imaged for 16h every 5 min, at oil-40X using an inverted video-microscope (Leica DMI6000) equipped with electron multiplying charge coupled device (EMCCD) camera controlled by Metamorph software (Molecular Devices). Images were mounted using Image J software.

Statistical analysis

In all graphs error bars represent the standard deviation (SD) from at least three independent experiments unless otherwise stated. Statistical significance of differences was calculated with Student's *t*-test or one/two-way ANOVA test with Tukey's multiple comparisons test, as indicated in the figure legends (ns: $p > 0.05$, * $p \leq 0.05$, ** $p \leq 0.01$, *** $p \leq 0.001$, **** $p \leq 0.0001$). All analyses were conducted using GraphPad Prism (version Mac OS X 7.0b).